^{54}Fe Neutron Elastic and Inelastic Scattering Differential Cross Sections from $2 - 6$ MeV

J.R. Vanhoy[a], S.H. Liu[b], S.F. Hicks[c], B.M. Combs[c], B.P. Crider[d], A.J. French[c], E.A. Garza[a], T. Harrison[a], S.L. Henderson[c], T.J. Howard[c], M.T. McEllistrem[d], S. Nigam[b], R.L. Pecha[c], E.E. Peters[b], F.M. Prados-Estévez[b], A.P.D. Ramirez[b], B.G. Rice[a], T.J. Ross[b], Z.C. Santonil[c], L.C. Sidwell[c], J.L. Steves[a], B.K. Thompson[a], S.W. Yates[b,d]

[a] *Dept. of Physics, United States Naval Academy, Annapolis, MD 21402, USA*
[b] *Dept. of Chemistry, University of Kentucky, Lexington, KY 40506, USA*
[c] *Dept. of Physics, University of Dallas, Irving, TX 75062, USA*
[d] *Dept. of Physics and Astronomy, University of Kentucky, Lexington, KY 40506, USA*

Abstract

Measurements of neutron elastic and inelastic scattering cross sections from ^{54}Fe were performed for nine incident neutron energies between 2 and 6 MeV. Measured differential scattering cross sections are compared to those from previous measurements and the ENDF, JENDL, and JEFF data evaluations. TALYS calculations were performed and modifications of the default parameters are found to better describe the experimental cross sections. A spherical optical model treatment is generally adequate to describe the cross sections in this energy region; however, in ^{54}Fe the direct coupling is found to increase suddenly above 4 MeV and requires an increase in the DWBA deformation parameter by approximately 25%. This has little effect on the elastic scattering differential cross sections but makes a significant improvement in both the strength and shape of the inelastic scattering angular distribution, which are found to be very sensitive to the size and extent of the surface absorption region.

Keywords: Neutron elastic and inelastic scattering, Differential cross sections, ^{54}Fe(n,n$'$), Coupled Channels, TALYS, ECIS06

Email addresses: vanhoy@usna.edu (J.R. Vanhoy), hicks@udallas.edu (S.F. Hicks)

1. Introduction

Iron is a ubiquitous material in buildings, laboratories, equipment, and devices. Because of its wide-spread usage, neutron-induced reactions on the iron isotopes have many different applications in engineering, physics, and medicine. The material properties of iron alloys such as strength, ductility, and long-term stability are determined by the defects in the material. The creation and growth of these defects depend on the elastic scattering differential cross sections and the (n,p) and (n,α) reaction rates.

Iron-54 is the second most abundant isotope in natural iron materials. Despite its only 5.5% natural abundance, the ^{54}Fe cross sections have a significant impact in fast reactor systems and energy transport and deposition in thick slabs of steel [1, 2].

The ^{54}Fe total cross sections in the fast neutron region do not show clear resonance behavior above $E_n \approx 2$ MeV, but they do fluctuate. These variations occur on a small energy scale, <0.1 MeV. In the 2 to 3 MeV energy range the average cross section is 3.39 b and the root-mean-square (rms) fluctuation is 0.57 b. In the energy range of 3 to 8 MeV the average cross section is 3.55 b and the rms fluctuation has dampened to 0.18 b. An optical model (OM) is used to describe the energy-averaged behavior of the cross sections.

While forward angle elastic scattering is dominated by diffraction that is well described by a range of OM parameters, the cross sections at angles $>120^o$ are much more sensitive to model details and must be measured to know accurate values. For example, the evaluated cross sections from ENDF, JENDL, and JEFF often disagree by factors of two to three on the large-angle elastic scattering cross sections and even more when inelastic neutron scattering cross sections are compared.

Elastic scattering cross sections are rather well measured for ^{54}Fe; previous experimental efforts are listed in Table 1. Inelastic experimental data are not so abundant, and modern inelastic scattering measurements on other nuclei indicate there can be significant discrepancies. In this work, we repeat mea-

surements of elastic and inelastic cross sections in the energy range 2 to 6 MeV and compare with databases, previous measurements, and model calculations. These newly measured inelastic scattering cross sections and their angular dependencies, provide the critical information that guides the choice of scattering potential parameters for direct-coupling collective models.

Table 1. Previous neutron scattering differential cross section measurements on ^{54}Fe.

Year	Author	Energies	Points/AD	Reference
1987	Korzh	5, 6, 7	13	[3]
1986	Guenther	36 btw 1.3-3.9	10	[4]
1982	El-Kadi	8, 10, 12, 14	26	[5]
1982	Delaroche	8, 10, 12, 14	26	[6]
1977	Korzh	1.5, 2, 2.5, 3	8	[7]
1974	Kinney	5.5, 7.0, 8.5	21	[8]
1973	Fedorov	2.9	8	[9, 10]
1971	Boschung	4.0, 5.0, 5.6	10	[11]
1967	Rogers	2.33	5	[12]

2. Methods

The equipment, methods, and data reduction techniques employed at the University of Kentucky Accelerator Lab are discussed extensively in several papers [13, 14, 15, 16]. The laboratory features a 7-MV single-ended model CN Van de Graaff with a terminal-based bunching system. The pulsed proton or deuteron beams have a time spread of Δt $\approx$ 1 ns at the neutron production target. The ^{3}H(p,n) and ^{2}H(d,n) reactions produce the fluence below and above 4.5 MeV neutron energy, respectively. The tritium or deuterium gas is held in a stainless steel gas cell 3 cm long and 0.8 cm in diameter. An entrance foil of 3.5 micron molybendum is used to separate the beamline vacuum from the $\sim$700 torr pressure in the cell. The cell is lined with tantalum foil and stopper

to prevent neutron production in the stainless steel. The stopper and foil are changed after approximately two weeks of beamtime. The energy spread of the neutrons impinging on each sample is approximately 75 keV at E_n = 3.5 MeV and 220 keV at 6 MeV.

Neutron production rates are recorded using time-of-flight (TOF) techniques with forward monitor (FM) detectors utilizing NE-213 or C_6D_6 scintillation fluids. A FM is placed at 45^o with respect to the incident beam direction and above the scattering plane to provide a direct, collimated view of the gas cell during all measurements. When ^{2}H(d,n) is used, a second FM is placed at 20^o because a minimum occurs in the neutron production cross section at 45^o. Source neutrons are identified in the FM by TOF and pulse-shape discrimination (PSD), the combination of which provides a very clean monitor of on-pulse neutron production.

Scattering samples were right circular cylinders hung 7.0 cm from the center of the gas cell. The ^{54}Fe sample was leased for 12 months from the U.S. National Isotope Development Program. The sample was 18.045 g of high-purity metal enriched to 97.6% ^{54}Fe cast into a cylinder 1.50 cm in diameter and height. Two polyethylene solid cylinders 1.94 cm × 2.41 cm and 0.96 cm × 1.49 cm (diameter × height) were used to measure ^{1}H(n,n) cross sections to compare to hydrogen cross section reference standards for absolute normalization. In addition, similarly sized samples of natural carbon and natural iron were employed for consistency checks.

Scattered neutrons were detected with an 11.5 cm diameter × 2.5 cm thick C_6D_6 liquid scintillator, which permitted PSD rejection of γ-ray events. This neutron detector was mounted on a carriage which can be rotated to cover scattering angles up to 155^o with respect to the incident beam direction. The carriage supports a full-length collimation system with flight paths up to 4 m. Example TOF spectra are shown in Fig. 1. Time widths (FWHM) of the elastic peak are 2.5 - 3.0 ns; this value is expected from the combination of beam pulse width, energy spread in the gas cell, and scintillator thickness.

The (n,n') reaction in the few-MeV energy range populates final states of

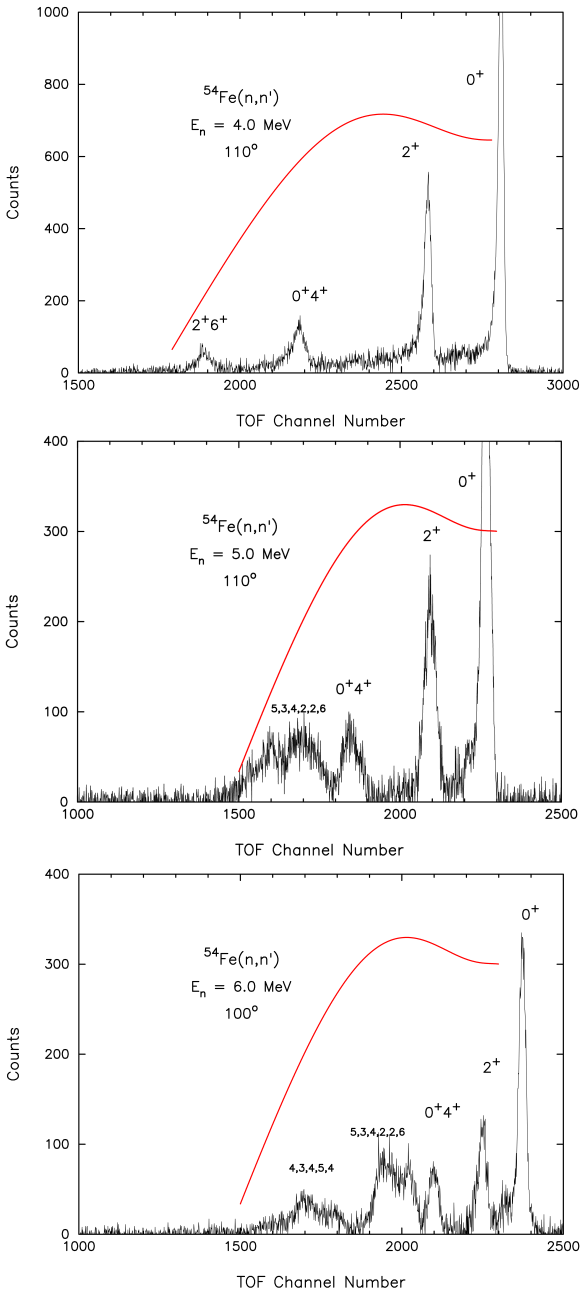

Figure 1: Example TOF spectra of neutrons scattered from ^{54}Fe at three selected energies. Background contributions have been subtracted. Peaks corresponding to population of various levels in ^{54}Fe are labeled. Relative detector efficiency curves are overlaid.

spins 0 to 6. The 1.408 MeV excitation energy of the 2_1^+ level places scattering from that exit channel well separated from the elastic scattering peak. Peaks from scattering to the 4_1^+ and 0_2^+ states of ^{54}Fe are unresolved in the TOF spectra since their excitation energies differ by only 23 keV. Also observed are two regions of unresolved peaks, with the first region containing scattering to levels between 2.9 and 3.4 MeV, and the second region for scattering to levels higher than 3.8 MeV in excitation energy. At $E_n = 4$ MeV, the efficiency and kinematics are such that only scattering from the close pair of levels at 2949-keV (6_1^+) and 2959-keV (2_2^+) appear in the higher-lying unresolved states, with most of the peak strength belonging to the 2^+ level. (The 2900-keV 2^+ level listed in ENSDF [17] is only reported in (e,e') [18] and is not considered.)

Peaks in the TOF spectra were fitted with SAN12, a program written in-house that allows for 6 variations in peak shape, selected from single, double, or asymmetric Gaussian and a exponential or linear tail. The most appropriate peak shapes for the present data were asymmetric Gaussian+exponential tail or double Gaussian+exponential tail. Parameters of the fitting function are generated from a reference peak, which is nearly always the elastic peak. Standard kinematic relations describe how peak positions, widths, and tails change within an individual TOF spectrum. To verify these peak shapes are appropriate for our gas cell - target combination, we ran MCNP simulations and tallied the attenuation and single, double, and triple scattering as a function of detector angle. The width and tailing parameters vary slightly with angle, but the peak shape and kinematic constraints mentioned above are correct.

For well-behaved data, the two fitting functions mentioned above give the same yields well within uncertainty. While the (n,n_1) peak is well separated from the elastic peak, care must be taken at the extreme forward angles to make sure strength from the strong elastic peak does not leak into the inelastic yield through the elastic peak's tail. The uncertainty of the (n,n_1) yield tends to grow at angles $<40^o$. In troublesome data sets, the first inelastic yield is extracted with a variety of model peak shapes and a best average value and uncertainty are chosen. This was not an issue for lower energy measurements. The concern

was most evident in the 3, 5, and 6 MeV data. For the 3 MeV data set, we rejected the forward angle cross section values entirely because the quality was not as good as all the other incident energies.

The C_6D_6 detector efficiency is determined by kinematics and direct measurement of the neutron source reaction angular distribution. This process is necessary because the sample and gas cell are close, and the neutron fluence emerging from the gas cell is divergent. The $d\sigma/d\Omega_{Tpn}$ cross sections are taken from the DROSG-2000 program series [19, 20]. Our cross section normalization technique is not sensitive to the magnitude of the ^{3}H(p,n) or ^{2}H(d,n) cross sections, only their angular dependence. Uncertainties in the angular dependence of these cross sections are one of the largest contributors to the overall uncertainty in the measured neutron scattering cross sections. The relative uncertainty in the angular variation is 3%.

Conversion to absolute cross sections is performed with reference to a hydrogen cross section standard. We use two sizes of polyethylene solid cylinders in order to check for issues arising from attenuation and multiple scattering corrections. Recommended values for the H(n,n) total cross sections are taken from Tables XVIII and XIX of Ref. [21] and Ref. [22], respectively. Both references provide the same absolute angle-integrated H(n,n) values which are known to $\pm$0.30% or better in our energy range. The differential cross sections in the center-of-mass system (CM) vary by $\pm$0.5% from the isotropic estimate, which is much smaller than the uncertainties incurred in $eff(E_n)$. Because of the small discrepancy, we consider $d\sigma/d\Omega$ to be isotropic in the center-of-mass frame.

Measured differential cross sections are corrected for attenuation and multiple scattering effects in the sample, taking into account the close cell-to-sample geometry with the code MULCAT [23]. The code performs an iterative Monte Carlo calculation, taking as input the uncorrected experimental differential cross sections and using them with known total cross sections and information on the ^{3}H(p,n) source reaction to estimate the corrected differential cross sections. MULCAT then repeats this process, using now the estimated cross sections as

input; the whole process is iterated until the differential cross sections converge. Uncertainties in the attenuation and multiple scattering corrections at angles greater than 70^o are typically 2 to 5%.

3. Observations

Representative experimental elastic scattering differential cross sections are shown in Figures 2 - 5 along with previous data and values from compilations. Experimental data are in good agreement at forward angles where the optical model direct contribution to the cross section is dominant. At larger angles the values between the data sets show scatter, which is consistent with the large rapid fluctuations noted previously in the compound cross sections at low energies. Above 3 MeV, the scatter between experimental data sets diminishes as the rapid fluctuations smooth out. The second diffraction minimum develops in the elastic scattering cross section above 3 MeV. However the upturn in large-angle elastic cross section predicted by the database evaluations (ENDF, JENDL, and JEFF) is not observed in the data, or at least not until after 150^o.

Representative experimental (n, n_1) inelastic scattering differential cross sections are shown in Fig. 6 along with previous data and values from compilations. The (n,n_1) angular distributions in the unresolved resonance region below 4 MeV are reasonably flat, as expected for compound nuclear processes. The inelastic peak yields at forward scattering angles are not significantly impacted by the large elastic peak in the TOF spectrum due to peak fitting ambiguities. If this were the case, there would be a distortion at forward angles. Between 2 and 3 MeV, the (n,n_1) differential cross sections lie between 45-55 mb/sr with little apparent structure. Above 3 MeV, the (n,n_1) compound-elastic contribution to the cross section drops noticeably due to competition with the other inelastic exit channels which are now open. The direct coupling contribution in the (n,n_1) channel becomes more apparent. For the $E_n = 5$ and 6 MeV data sets, a forward-angle enhancement of the differential cross section is apparent even in the raw online TOF spectra before analysis.

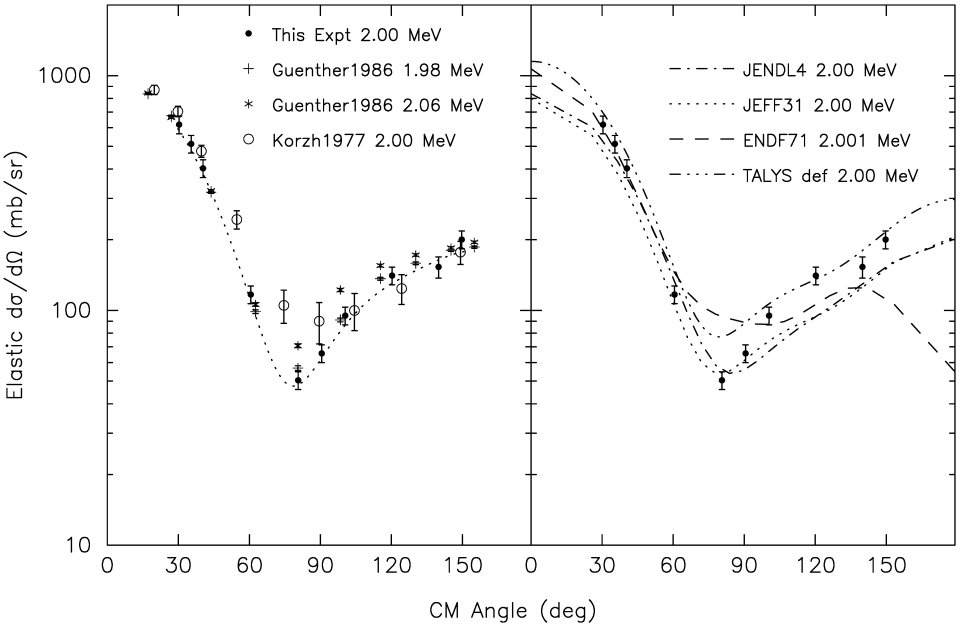

Figure 2: Comparison of measured 2.00 MeV elastic scattering cross sections (solid points with uncertainties) to previous data (left) and the evaluated nuclear libraries (right). The shape of $d\sigma/d\Omega$ changes quickly with energy at angles $>80^o$. Rapid changes at large angles are consistent with the compound nuclear resonance structure. The TALYS def curve is a calculation using the default RIPL parameters [24], without modification.

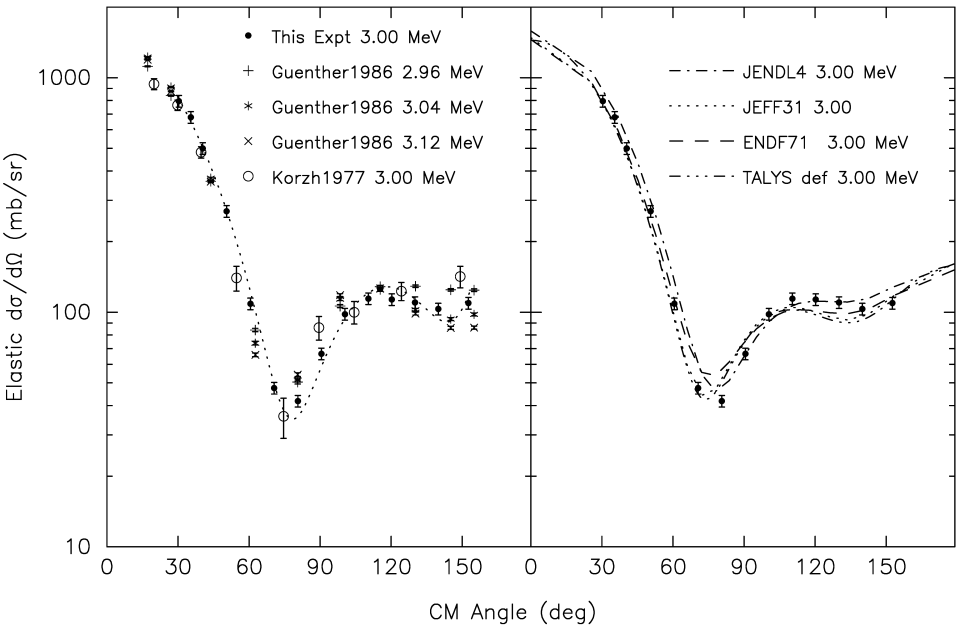

Figure 3: Comparison of measured 3.00 MeV elastic scattering cross sections (solid points with uncertainties) to previous data (left) and the evaluated nuclear libraries (right). Above 3 MeV, the scatter between experimental data sets diminishes as the rapid fluctuations in the total cross section diminish.

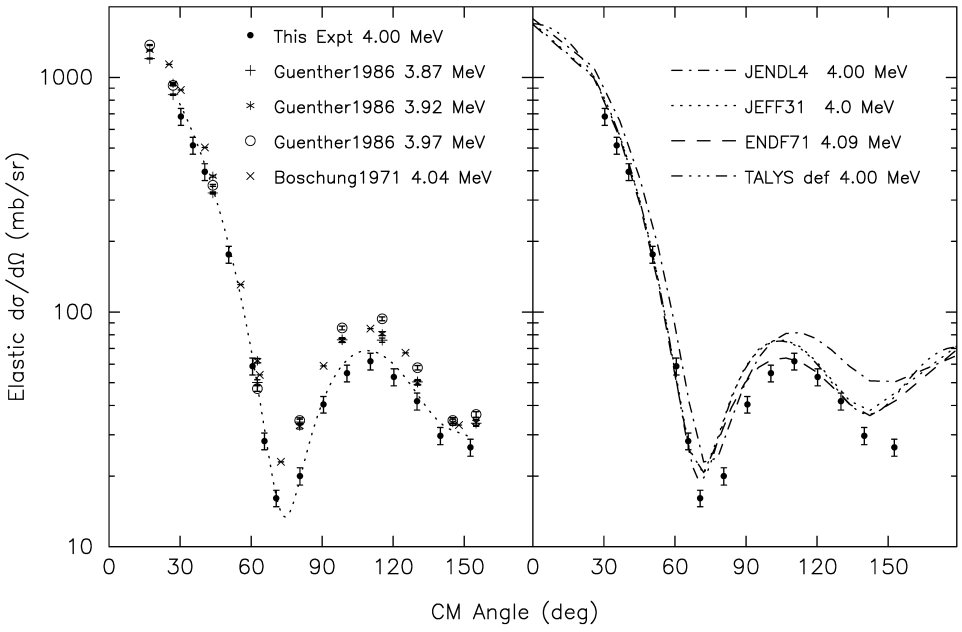

Figure 4: Comparison of measured 4.00 MeV elastic scattering cross sections (solid points with uncertainties) to previous data (left) and the evaluated nuclear libraries (right). Scatter between measurements at nearby energies diminishes, which is consistent with the smoothing of the compound cross section.

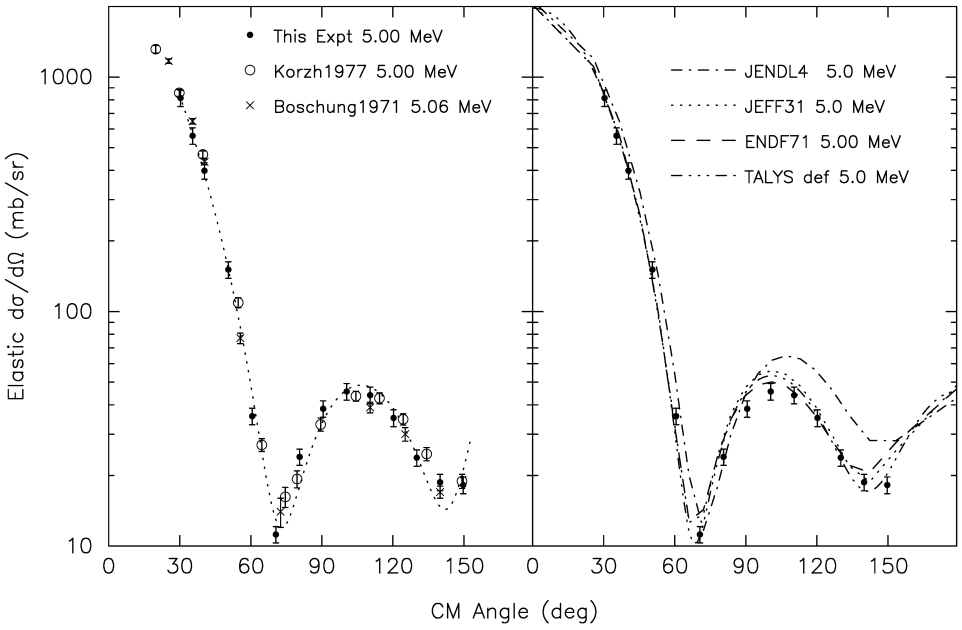

Figure 5: Comparison of measured 5.00 MeV elastic scattering cross sections (solid points with uncertainties) to previous data (left) and the evaluated nuclear libraries (right). Although no data exist at angles $>150^o$ the location of the second minimum is experimentally defined.

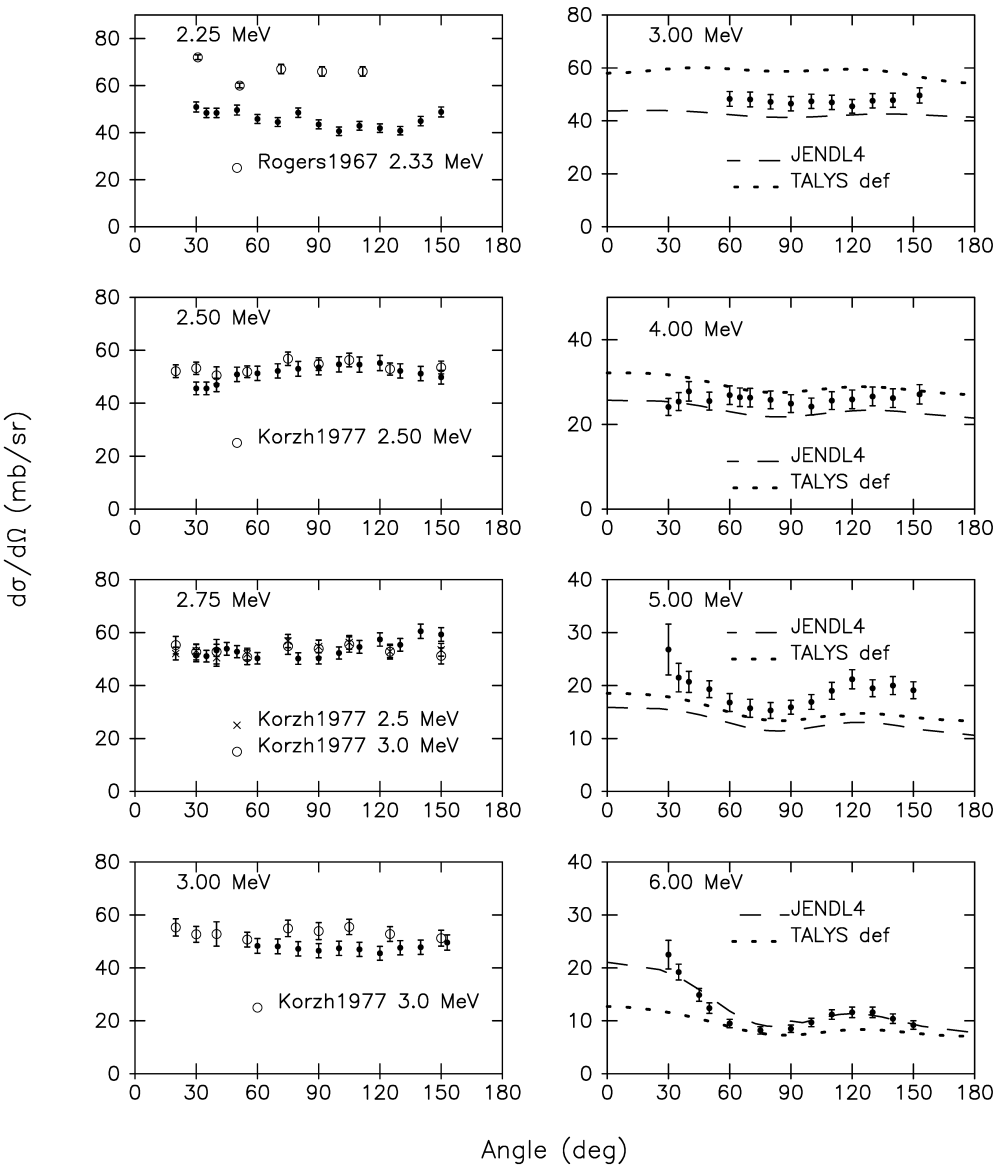

Figure 6: Comparison of measured (n,n_1) scattering cross sections (solid points with uncertainties) to previous data (left) and the evaluated nuclear libraries (right). Inelastic cross sections below 4 MeV can be explained by the compound mechanism; direct coupling suddenly increases in importance above 4 MeV.

Peaks corresponding to the population of the 2538-keV 4_1^+ and 2561-keV 6_1^+ levels are not resolvable in the TOF spectrum although the 23 keV energy difference does produce noticeable distortion in the shape. The measured scattering angular distributions to these levels are not remarkable and therefore not shown in a figure.

4. Interpretation

Although the total neutron scattering cross section clearly indicates strong fluctuations from indefineable overlapping resonances, the angular distributions in the elastic channel still show the classic diffraction shapes and therefore contain information on strengths and radii of the average potential along with direct coupling strengths.

While a spherical optical model treatment may intially provide a reasonable description, better quality calculated differential cross sections may occur when shape details of the interaction potential, the nature of the collective effects, and the form of the kinetic energy operator reflect the actual particles and nuclei involved.

The nucleus ^{54}Fe with N = 28 is not expected to be significantly deformed and excitations are expected to be dominated by the proton hole pairs and particle-hole excitations of the neutrons. Indeed, the low-lying nuclear structure of ^{54}Fe is strongly suggestive of bands built upon 2-particle structures: the 0, 2, 4, 6 ground band of the $\pi f_{7/2}^{-2}$; the 0_2^+ a $\nu(2p-2h)$ bandhead; and the remaining sequence controlled by $\nu(1p-1h)$ and $\nu p_{3/2}^{-1} \otimes f_{7/2}^{-1}$ configurations [25, 26, 27]. The g-factor measurements by East [28] also reinforce the strong proton configuration of the 2_1^+ level.

Cross sections in the ENDF/B-VII database [29] below 20 MeV are ultimately taken directly from the ENDF/B-VI.1 calculations [30, 31] which used a DWUCK4 DWBA approach and the Hauser-Feshbach code TNG [32, 33, 34]. Additional details of the calculation are not readily available.

The JENDL-4.0 database uses a standard neutron spherical optical model

approach and a coupled channel calculation but details are not readily available [35, 36, 37]. The JENDL database presents cross sections to the individual inelastic channels and we have used them in many of the previous figures.

The JEFF-3.1 database for ^{54}Fe [38] was constructed with the nuclear model code TALYS [39], version 0.56, with slight changes to some default parameters. The DWBA approach was used for inelastic scattering. A fairly complete description of the calculation is found in the database's information file.

4.1. Sensitivity to Optical Model Parameter Changes

Realistic calculations for cross sections, particularly for the inelastic channels, requires inclusion of all open reaction channels in order to appropriately distribute the available reaction strength. Neglecting open channels will lead to an over estimation of specific inelastic scattering cross sections. The (n,p) channel, with Q = +0.085 MeV, becomes significant above E_n = 2 MeV and increases to 30% of the reaction strength. The (n,α) channel, with Q = +0.843 MeV, is also open but its importance is strongly suppressed because of the Coulomb barrier. Optical model parameter sets are often developed from data in the energy range above 8 MeV and there can be issues when extrapolating those calculations down into the few-MeV region where the compound elastic process is significant.

The extensive measurements by Guenther below E_n = 4 MeV were well explained by a spherical optical model treatment [4]. The angular distributions of the (n,n_1) channel displayed in Fig. 6 clearly indicate the onset of direct reaction strength above 4 MeV. This forward angle enhancement of the (n,n_1) angular distribution persists until just above 14 MeV and disappears by 17 MeV when data from other groups are considered [5, 40, 41].

TALYS is a very convenient tool to perform optical model and coupled channels calculations as it manages all open channels that are so important for a nucleus such as ^{54}Fe. The form of the neutron potential is

$$U(r,E) = -V_V(E)f(r,R_V,a_V) - iW_V(E)f(r,R_V,a_V)$$

$$
\begin{aligned}
&+i4a_D W_D(E)\frac{d}{dr}f(r,R_D,a_D)\\
&+V_{SO}(E)(\frac{\hbar}{m_\pi c})^2\frac{1}{r}\frac{d}{dr}f(r,R_{SO},a_{SO})\ell\cdot\sigma\\
&+iW_{SO}(E)(\frac{\hbar}{m_\pi c})^2\frac{1}{r}\frac{d}{dr}f(r,R_{SO},a_{SO})\ell\cdot\sigma \qquad (1)
\end{aligned}
$$

where the function f is the standard Woods-Saxon form factor with radius R and diffuseness a, and V_V, W_V, W_D, V_{SO}, and W_{SO} are the strengths of the volume V, surface derivative D, and spin-orbit SO potentials. All potential strengths are energy dependent with parameterizations given in the TALYS manual. Note that the volume absorption term W_V uses the volume radius and diffuseness while the surface absorption term W_D uses a different radius and diffuseness.

In general, the default TALYS parameters [24] do an excellent job with the elastic scattering differential cross sections. Two parameter sets are provided: one for a spherical optical model calculation and another intended for use with the dispersion correction approach. Both parameter sets treat the inelastic channels with a spherical DWBA approach and give nearly identical results in our energy range.

We examined perturbations of the default parameters to gain understanding of the reaction mechanism for n + ^{54}Fe. Elastic scattering is well described with the default parameter set, but the strength of the (n,n_1) channel is weak at 5 and 6 MeV. Adjustments to the volume absorptive potential have no significant impact upon the (n,n_0) and (n,n_1) channels. Adjustments to the strength of the surface absorption W_D do not significantly improve the inelastic channel and spoil the agreement for the elastic angular distribution. The (n,n_0) and (n,n_1) channels are very sensitive to the radial location of the surface absorption. One can make improvements to the inelastic channel by increasing the surface derivative diffuseness a_D up to 25% and slightly lowering r_D: however this harms the minima in the elastic diffraction pattern. The best solution is to simply raise the DWBA deformation parameter (originally equivalent to $\beta_2 = 0.19$) by up to 50%. This adjustment spreads the region over which the surface

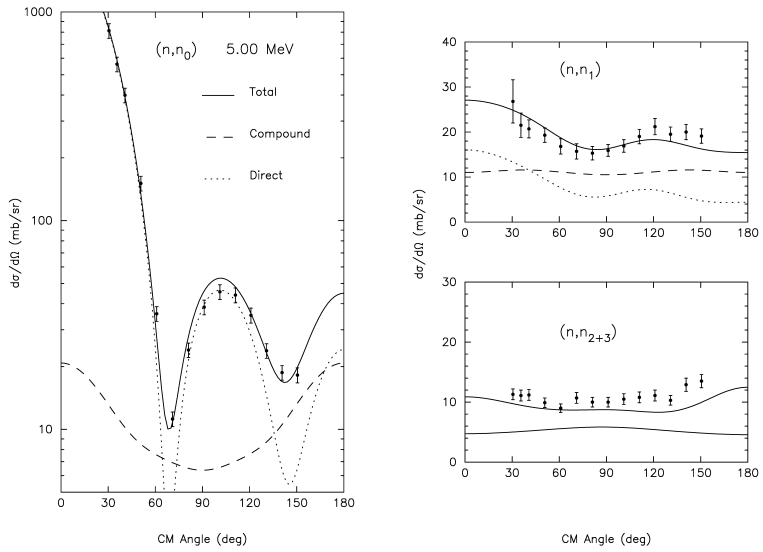

Figure 7: Neutron angular distributions at 5 MeV with modified TALYS parameters. The compound and direct contributions are indicated for the elastic and first inelastic cross sections. Increasing the DWBA deformation parameter provides substantial improvement to the (n,n$_1$) channel. The peaks corresponding to population of the 0_2^+ and 4_1^+ states are not resolved in the TOF spectra, but the summed measured angular distribution is adequately represented by the summed model calculation.

absorption acts because the nuclear radius $R(\theta, \phi) = R_o[1 + \beta_2 Y_{2,0}(\theta, \phi)]$ now varies with location about the nucleus. TALYS also applies this deformation to the central and volume absorptions terms, but it does not generate a significant impact upon the elastic scattering angular distribution for reasons discussed previously. There is a large improvement in both the strength and shape of the inelastic angular distribution. This better solution for 5 MeV is shown in Fig 7. The same procedure applied to the 6 MeV data leads to very similar conclusions and produces the solution shown in Fig. 8, but with the DWBA deformation parameter increased by 25%.

At 5 and 6 MeV, the first minimum in the (n,n_1) angular distribution occurs at a smaller angle than indicated in the calculation, suggesting the surface

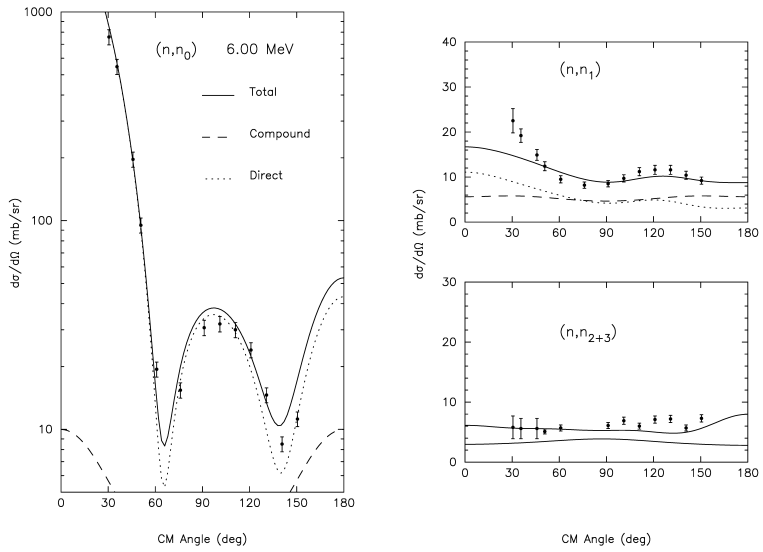

Figure 8: Neutron angular distributions at 6 MeV with modified TALYS parameters. The compound and direct contributions are indicated for the elastic and first inelastic cross sections. Minima in the elastic angular distribution are more apparent than at 5 MeV because the compound elastic strength has dropped significantly. Increasing the DWBA deformation parameter again provides substantial improvement to the (n,n_1) channel.

absorption should be positioned at a slightly greater average radius. We were unable to alter radial, diffuseness, or absorption OMP parameters to solve this issue without damaging the agreement in the elastic channel.

These larger values for the deformation parameter demonstrate that ^{54}Fe exhibits strong enough collective behavior that a coupled-channels calculation is warranted. A spherical optical model with a vibrational perturbation is likely the most appropriate. We allow coupling to the 2_1^+, 4_1^+ , and 0_2^+ states and manage these ECIS calculations via the TALYS front end. Again, the quadrupole phonon coupling parameter had to be increased by $\sim$25% and results were equivalent to the simple DWBA treatment discussed previously, including the problem with the first minimum in the first-inelastic angular distribution.

Neutron scattering investigations of the neighboring nucleus ^{56}Fe [42] indicate a soft rotor model is necessary due to the rotation-vibration collectivity present in the lower-lying levels [6, 43, 41]. A simpler description may be adequate for ^{54}Fe because of the particle-pair excitation structures described above. Iron-54 was examined within the soft-rotor model by Li [41], but at higher energies than in this study: $E_n > 7$ MeV for elastic scattering and $E_n > 14$ MeV for the (n,n_1) channel. That calculation does a very nice job of managing all of the open exit channels (n,n), (n,p), and (n,α), but deviations from data are observed at the lowest energies considered.

5. Summary

Neutron scattering angular distributions were measured for 9 incident neutron energies between 2 and 6 MeV.

Most general optical model discussions suggest the balance between volume and surface terms is not so observable, but for ^{54}Fe there is a pronounced effect. It is not surprising that the absorption would be surface-dominant at lower energies, but the effect is typically not observable in most other nuclei.

The DWBA deformation parameter for neutron excitation of the first excited state in ^{54}Fe is closer to that of ^{56}Fe than previously thought. Initially this might seem surprising, since the electromagnetic decay strengths of the first 2^+ levels of the two nuclei are different; however, this indicates that electromagnetic decays provide guidance about the nuclear structure of levels, but do not provide specific information about the nature of the direct excitation mechanism through the strong nuclear force. This effect is observed in other nuclei such as ^{48}Ca [44, 45] and ^{204,206}Pb [46].

6. Acknowledgments

Research at the University of Kentucky Accelerator Laboratory is supported by contracts from the U.S. Department of Energy NNSA-SSAP award NA-0002931 and Nuclear Energy Universities Program award NU-12-KY-UK-0201-

05, the U.S. National Isotope Development Program, and the Cowan Physics Fund at the University of Dallas. The authors also acknowledge the many contributions of H.E. Baber to these measurements.

[1] M.Schulc, M.Kostal, D.Harutyunyan, P.Baron, E.Novak, Applied Radiation and Isotopes 128 (2017) 86 – 91. doi:10.1016/j.apradiso.2017.06.025.

[2] B.Jansky, J.Rejchrt, E.Novak, E.Losa, A.I.Blokhin, E.Mitenkova, E.J.P. Web Conf 146 (2017) 06021. doi:10.1051/epjconf/201714606021.

[3] I.A.Korzh, V.A.Mishchenko, N.M.Pravdivy, Atomnaya Energiya 62 (6) (1987) 417.

[4] P.T.Guenther, D.L.Smith, A.B.Smith, J.F.Whalen, Annals of Nuclear Energy 13 (11) (1986) 601. doi:10.1016/0306-4549(86)90017-4.

[5] S.M.El-Kadi, C.E.Nelson, F.O.Purser, R.L.Walter, A.Beyerle, C.R.Gould, L.W.Seagondollar, Nucl. Phys. A 390 (3) (1982) 509. doi:10.1016/0375-9474(82)90281-0.

[6] J.P.Delaroche, S.M.El-Kadi, P.P.Guss, C.E.Floyd, R.L.Walter, Nucl. Phys. A 390 (3) (1982) 541. doi:10.1016/0375-9474(82)90282-2.

[7] I.A.Korzh, V.A.Mishchenko, E.N.Mozhzhukhin, N.M.Pravdivij, I.E.Sanzhur, Ukrainskii Fizichnii Zhurnal 22 (1977) 87.

[8] W.E.Kinney, F.G.Perey, ^{54}Fe neutron elastic and inelastic scattering cross sections from 5.50 to 8.50 MeV, Tech. Rep. 4907, ORNL (Feb. 1974).

[9] M.B.Fjodorov, T.I.Jakovenko, N.T.Surovitskaja, E.B.Korbetskij, L.S.Sokolov, Second Conference on Neutron Physics 3 (1973) 56.

[10] M.B.Fjodorov, T.I.Jakovenko, N.T.Surovitskaja, E.B.Korbetskij, L.S.Sokolov, Ukrainskii Fizichnii Zhurnal 20 (3) (1974) 384.

[11] P.Boschung, J.T.Lindow, E.F.Shrader, Nucl. Phys. A 161 (2) (1971) 593. doi:10.1016/0375-9474(71)90388-5.

[12] W.L.Rodgers, E.F.Shrader, J.T.Lindow, Tech. Rep. 1573, Chicago Operations Office, A.E.C. (1967).

[13] J.R.Vanhoy, S.F.Hicks, H.E.Baber, B.P.Crider, E.E.Peters, F.M.Prados-Estvez, T.J.Ross, M.T.McEllistrem, S.W.Yates, Basic and Applied Science Using Monoenergetic Pulsed Neutron Beams from the University of Kentucky Accelerator Laboratory, in Proceedings of the AccApp13 Conference, Brugge, 5-8 August 2013.

[14] J.R.Vanhoy, S.F.Hicks, B. Champine, B.P.Crider, E.Garza, S.L.Henderson, S.H.Liu, E.E.Peters, F.M.Prados-Estevez, M.T.McEllistrem, T.J.Ross, L.C.Sidwell, J.Steves, S.W.Yates, Differential Cross Sections Measurements at the University of Kentucky Accelerator Adventures in Analysis , Tech. Rep. 13, NEMEA-7 / CIELO, NEA/NSC/DOC (2014).

[15] J.R.Vanhoy, S.F.Hicks, A.Chakraborty, B.R.Champine, B.M.Combs, B.P.Crider, L.J.Kersting, A.Kumar, C.J.Lueck, S.H.Liu, P.J.McDonough, M.T.McEllistrem, E.E.Peters, F.M.Prados-Estevez, L.C.Sidwell, A.J.Sigillito, D.W.Watts, S.W.Yates, Nucl. Phys. A 939 (2015) 121. doi:10.1016/j.nuclphysa.2015.03.006.

[16] P.E.Garrett, N.Warr, S.W.Yates, J. Res. Natl. Inst. Stand. Technol. 105 (2000) 141. doi:10.6028/jres.105.019.

[17] Y. Dong, H. Junde, Nuclear Data Sheets 121 (2014) 1. doi:10.1016/j.nds.2014.09.001.

[18] J. Bellicard, P. Barreau, Nucl. Phys. 36 (1962) 476. doi:10.1016/0029-5582(62)90471-6.

[19] M.Drosg, Drosg-2000: Neutron Source Reactions and Codes DROSG-2000 of the IAEA version 2.21, Tech. Rep. IAEA-NDS-87 Rev. 8, IAEA (2003).

[20] H. Liskien, A. Paulsen, At. Data and Nucl. Data Tables 11 (7) (1973) 569. doi:10.1016/S0092-640X(73)80081-6.

[21] A.D.Carlson, V.G.Pronyaev, D.L.Smith, N.M.Larson, Z. Chen, G.M.Hale, F.-J.Hambsch, E.V.Gai, S.-Y. Oh, S.A.Badikov, T.Kawano, H.M.Hofmann, H.Vonach, S.Tagesen, Nuclear Data Sheets 110 (12) (2009) 3215. doi:10.1016/j.nds.2009.11.001.

[22] G.M.Hale, ENDF/V-II.1 ^{1}H(n,n) Reaction Evaluation, Tech. rep., LANL (Dec. 2006).

[23] J.R.Lilley, MULCAT-BRC, A Monte Carlo Neutron and Gamma-Ray Multiple Scattering Correction Program, Tech. Rep. P2N/934/80, Internal Service de Physique et Techniques Nucleaire, Centre dEtudes de Bruyeres-le-Chatel (1980).

[24] R.Capote, M.Herman, P.Obloinskii, P.G.Young, S.Goriely, T.Belgya, A.V.Ignatyuk, A.J.Koning, S.Hilaire, V.A.Plujko, M.Avrigeanu, O.Bersillon, M.B.Chadwick, T.Fukahori, Z. Ge, Y. Han, S.Kailas, J.Kopecky, V.M.Maslov, G.Reffo, M.Sin, E.Sh.Soukhovitskii, P.Talou, Nuclear Data Sheets 110 (12) (2009) 3107. doi:10.1016/j.nds.2009.10.004.

[25] T. Suehiro, J. Kokame, Y. Ishizaki, H. Ogata, Y. Sugiyama, Y. Saji, I. Nonaka, K. Itonaga, Nuclear Physics A 220 (3) (1974) 461. doi:10.1016/0375-9474(74)90128-6.

[26] R. F. Casten, E. R. Flynn, O. Hansen, T. J. Mulligan, Phys. Rev. C 4 (1971) 130. doi:10.1103/PhysRevC.4.130.

[27] P. David, H.H.Duhm, R. Bock, R. Stock, Nucl. Phys. A 128 (1) (1969) 47. doi:10.1016/0375-9474(69)90978-6.

[28] M. C. East, A. E. Stuchbery, S. K. Chamoli, J. S. Pinter, H. L. Crawford, A. N. Wilson, T. Kibédi, P. F. Mantica, Phys. Rev. C 79 (2009) 024304. doi:10.1103/PhysRevC.79.024304.

[29] M.B.Chadwick, P.G.Young, D.Hetrick, ^{54}Fe LANL-ORNL Evaluation of Sept 1996, distribution Dec 2006, Revision 4 of 22 Dec 2011, Tech. rep., LANL-ORNL (Sep. 1996).

[30] D.M.Hetrick, C.Y.Fu, N.M.Larson, ENDF/B-VI.1 Evaluation of n + ^{54}Fe, Tech. rep. (1991).

[31] C.Y.Fu, D.M.Hetrick, Report ORNL/TM-9964, ENDF-341^{54}Fe LANL-ORNL Evaluation of Sept 1996, distribution Dec 2006, Revision 4 of 22 Dec 2011, Tech. rep., ORNL (1986).

[32] C.Y.Fu, Report ORNL/TM-7042A Consistent Nuclear Model For Compound and Pre- compound Reactions with Conservation of Angular Momentum, Tech. rep., ORNL (1980).

[33] C.Y.Fu, report BNL-NCS-51425Development and Application of Multistep Hauser-Feshbach/Pre-equilibrium Model Theory," Symp. Neutron Cross Sections from 10 to 50 MeV , Tech. rep., BNL (1980).

[34] K.Shibata, C.Y.Fu, Report ORNL/TM-10093 Recent Improvements of the TNG Statistical Model Code, Tech. rep., ORNL (1986).

[35] K. Shibata, S. Iijima, H. Yamakoshi, JENDL-4.0 Evaluation of n + ^{54}Fe, 4 Sept 2009, Distribution of May 2010, Tech. rep., JAEA (2009).

[36] E.M.Cornelis, L.Mewissen, F.Poortmans, Proc. Int. Conf. Nuclear Data for Science and Technology, Antwerp 1982 (1983) 135doi:10.1007/978-94-009-7099-1_26.

[37] S. Igarasi, J. Nucl. Sci. Technol. 12 (1975) 67. doi:10.1080/18811248.1975.9733073.

[38] A.J.Koning, M.C.Duijvestijn, ^{54}Fe JEFF-3.1 Evaluation of Oct 2004, distribution May 2005, Revision 1, Tech. rep., NRG Petten (May 2005).

[39] A.J.Koning, S.Hilaire, M.C.Duijvestijn, Proceedings of the International Conference on Nuclear Data for Science and Technology (2008) 21122-27 April 2007, Nice, France, editors O.Bersillon, F.Gunsing, E.Bauge, R.Jacqmin, and S.Leray, EDP Sciences.

[40] S. Mellema, R. W. Finlay, F. S. Dietrich, Phys. Rev. C 33 (1986) 481. doi:10.1103/PhysRevC.33.481.

[41] R. Li, W. Sun, E. S. Soukhovitskiĭ, J. M. Quesada, R. Capote, Phys. Rev. C 87 (2013) 054611. doi:10.1103/PhysRevC.87.054611.

[42] A. P. D. Ramirez, J. R. Vanhoy, S. F. Hicks, M. T. McEllistrem, E. E. Peters, S. Mukhopadhyay, T. D. Harrison, T. J. Howard, D. T. Jackson, P. D. Lenzen, T. D. Nguyen, R. L. Pecha, B. G. Rice, B. K. Thompson, S. W. Yates, Phys. Rev. C 95 (2017) 064605. doi:10.1103/PhysRevC.95.064605.

[43] E. S. Sukhovitskii, S. Chiba, J.-Y. Lee, B. t. Kim, S.-W. Hong, Journal of Nuclear Science and Technology 40 (2) (2003) 69. doi:10.1080/18811248.2003.9715335.

[44] S. F. Hicks, S. E. Hicks, G. R. Shen, M. T. McEllistrem, Phys. Rev. C 41 (1990) 2560. doi:10.1103/PhysRevC.41.2560.

[45] J. R. Vanhoy, M. T. McEllistrem, S. F. Hicks, R. A. Gatenby, E. M. Baum, E. L. Johnson, G. Molnár, S. W. Yates, Phys. Rev. C 45 (1992) 1628. doi:10.1103/PhysRevC.45.1628.

[46] S. F. Hicks, J. M. Hanly, S. E. Hicks, G. R. Shen, M. T. McEllistrem, Phys. Rev. C 49 (1994) 103–115. doi:10.1103/PhysRevC.49.103.